Ultra-Narrow Band Blue Emission of Eu^{2+} in Halogenated (Alumino)borate Systems Based on High Lattice Symmetry

Yi Wei, [†] Xingyu Qu, [†] Jiarui Hao, [†] Guogang Li, [*, †] Sisi Liang, [‡] Peipei Dang, [‡] Ziyong Cheng, [*, ‡] Maxim S. Molokeev, [§, Δ, #] Chun Che Lin, [&] Ting-shan Chan, [∏] and Jun Lin [*, ‡, ◊]

† Engineering Research Center of Nano-Geomaterials of Ministry of Education, Faculty of Materials Science and Chemistry, China University of Geosciences, 388 Lumo Road, Wuhan 430074, P. R. China. Email: ggli@cug.edu.cn

‡ State Key Laboratory of Rare Earth Resource Utilization, Changchun Institute of Applied Chemistry, Chinese Academy of Sciences, Changchun 130022, P. R. China. Email: jlin@ciac.ac.cn

§ Laboratory of Crystal Physics, Kirensky Institute of Physics, SB RAS, Krasnoyarsk 660036, Russia

Δ Department of Physics, Far Eastern State Transport University, Khabarovsk, 680021 Russia

 # Siberian Federal University, Krasnoyarsk, 660041, Russia.

& Institute of Organic and Polymeric Materials, National Taipei University of Technology, Taipei 106, Taiwan.

∏ National Synchrotron Radiation Research Center, Hsinchu 300, Taiwan.

◊ School of Applied Physics and Materials, Wuyi University, Jiangmen, Guangdong, 529020, P. R. China.

ABSTRACT: Phosphor materials with ultra-high color purity are highly desired in backlit display of various light-emitting devices. How to achieve high-purity three-primary emission in rare earth ions activated inorganic phosphors has become a hot topic of research. Herein, we reported extremely narrow band and highly efficient blue-violet-emitting Eu^{2+}-doped $Ba_2B_5O_9X$ (fwhm = 31 nm) and $NaBa_4(AlB_4O_9)_2X_3$ (X = Cl, Br) (fwhm = 43 nm) phosphors with peak positions around 424–437 nm. Especially, the 31 nm-fwhm $Ba_2B_5O_9Cl$:Eu sample is the narrowest one among the reported rare earth doped blue-emitting phosphors, whose color purity even exceeded 97%. The EXANES analysis revealed that the Eu mainly existed in the form of +2. The extraordinarily narrow band emission has been analyzed according to the Rietveld structural refinement, which should be attributed to the highly symmetric lattice structures with the flower-like polyhedrons in the studied (alumino)borate matrixes. Significantly, the color gamut of as-prepared blue phosphors combined with the standard green and red phosphors was almost close to that of Rec. 2020 display standards. Finally, the electroluminescence performances of the studied phosphors in WLEDs devices were systematically investigated, which present low color correlated temperatures (CCT = 2578 - 4836 K), high color rendering indexes (Ra = 91.2- 97.6) and high luminescence efficiency (around 13.40 lm/W). All these results demonstrate that the as-prepared phosphors could be superior blue-emitting candidates for backlit display as well as WLEDs.

■ INTRODUCTION

In recent years, rare earth ions activated inorganic phosphor materials have been extensively reported and applied in white light emitting diodes (WLEDs) lighting and backlit display devices due to their outstanding stability, high yield, low cost and environmental friendliness.[1-6] How to achieve highly efficient and highly pure three-primary emission of phosphors has become a hot topic of research. Up to now, the most reported promising materials for backlit display are the novel perovskites quantum dots with high luminescence intensity and narrow full width at half maximum (abbreviated as fwhm) of 12-42 nm.[7-9] However, the perovskites quantum dots have an issue of terrible stability and moisture tolerance, which limits their application for backlit display and WLEDs.[10-11] Therefore, traditional rare earth activated inorganic phosphor materials with high color purity have drawn many attention to applying in backlit display as well as WLEDs. For examples, some previous reports have a new perspective that the highly symmetric lattice structure in could generate a narrow fwhm. Zhang et al.[12] reported a green emitting β‑SiAlON:Eu with narrow emission band (fwhm = 49 nm), which Eu^{2+} ions occupy a highly rigid hexagonal channel. Braun et al.[13] reported layered-structure $M_3Si_6O_{12}N_2$:Eu^{2+} with highly pure green emission (fwhm = 65 nm). Li et al.[14] presented novel narrow-band blue and cyan-emitting $(Sr_{1-x}Ba_x)Si_2O_2N_2$:Eu^{2+} phosphors by occupying highly symmetry Ba^{2+} cuboid sites. Those studies reveal that the highly symmetric lattice structure trends to form a highly pure narrow-band emission. Therefore, to explore phosphors with highly symmetric lattice structure could extend their application in the field of backlight display.

On the other hand, given the sensitivity to the coordination environment, controllable emission of Eu^{2+} ions could be expected by appropriately modifying host lattice in

solid solution compounds. Among them, cation substitution strategy has drawn many attention for designing novel phosphor materials and optimizing the luminescence properties by adjusting the local lattice structure.[15-16] For examples, Xia et al.[17] reported a chemical unit co-substitution way to adjust luminescence in $Ca_2(Al_{1-x}Mg_x)(Al_{1-x}Si_{1+x})O_7:Eu^{2+}$ phosphor. Wang et al.[18] designed a green emitting $Ca_{2-x}Y_{1+x}Zr_{-x}Al_{3+x}O_{12}:Ce^{3+}$ solid solution by [CaZr-YAl] cation co-substitution. Zhang et al.[19] discovered blue-emitting $Li_4Sr_{1+x}Ca_{0.97-x}(SiO_4)_2:Ce^{3+}$ phosphors with high quantum efficiency by [Ca-Sr] cation substitution. These researches mainly focus on changing the local structure environment around activators ions for adjusting the profile of the emission spectra, including emission intensity and emission peak position and. However, the adjustment of fwhm via cation substitution strategy has not been systematically investigated, and the corresponding mechanism urgently need to be explored and revealed.

Highly efficient blue-emitting phosphors are indispensable and highly desired in tricolor phosphors based WLEDs and backlit display. Especially, the high pure blue phosphor is necessary for backlit display. However, the commercially available blue phosphor such as $BaMgAl_{10}O_{17}:Eu^{2+}$ (BAM:Eu^{2+}) could not completely meet the color purity requirement of backlit display due to the large fwhm.[20-23] Another reported blue emitting phosphors have either inapposite excited position or broad band, which are also not extensively applied in backlit display. Therefore, the design of highly efficient blue phosphors with high color purity is urgent for the further development of backlit display and WLED devices. Recently, Lian et al.[24] discovered a novel Eu^{2+}-doped $NaBa_4(AlB_4O_9)_2X_3$ (X = Cl, Br) phosphors with high efficient blue emission and high color purity (fwhm = 33-37 nm), but it's intrinsic mechanism for high color purity is unclear, which need to be revealed. In our previous work, we reported a $BaAl_{12}O_{19}:Eu^{2+}$ phosphor with superior thermal stability and high color purity (fwhm = 52 nm) by programing Eu^{2+} ions to enter into highly symmetric Ba^{2+} lattice sites.[25] Therefore, we are dedicated to arranging Eu^{2+} in a high symmetry environment to realize a narrow band blue emission and clarify the implied mechanism. In this work, we employed two kind of crystal structures named $Ba_2B_5O_9X$ and $NaBa_4(AlB_4O_9)_2X_3$ (X = Cl, Br) (aliased as BBOC:Eu, BBOB:Eu, NBAC:Eu, NBAB:Eu, respectively) with highly symmetric lattice structure, notably, the two crystal structures are almost the same but belong to different crystal phases and space groups. Phase transformation could be clearly obtained by cation substitution of $[AlO_4] \rightarrow [BO_4]$. Interestingly, Eu^{2+} ions realized highly efficient blue-violet emission as well as ultra-narrow emission (fwhm = 31-43 nm) in $Ba_2B_5O_9X$ and $NaBa_4(AlB_4O_9)_2X_3$ (X = Cl, Br) hosts. Significantly, the color gamut of as-prepared blue phosphors combined with the standard green and red phosphors was almost close to that of Rec. 2020 display standards, which suggested that the as-prepared blue phosphors are the superior candidates for application in backlit display area. Finally, the relationship between lattice symmetry and narrow emission band has been systematically investigated and revealed.

■ EXPERIMENTAL SECTION

Materials synthesis. $Ba_2B_5O_9X:Eu^{2+}$ and $NaBa_4(AlB_4O_9)_2X_3:Eu^{2+}$ (X = Cl, Br) phosphor powders were synthesized via high temperature solid-state routes. The doping concentration of Eu^{2+} ions was fixed at 10 mol% of the content of Ba^{2+} ions in the host. Na_2CO_3 (99.8%), $BaCl_2 \cdot 2H_2O$ (99.5%), Al_2O_3 (99.99%), H_3BO_3 (99.5%), Eu_2O_3 (≥ 99.99%) and $BaBr_2$ (99%) were used as raw materials. All the reagents except Eu_2O_3 and $BaBr_2$ were purchased from Sinopharm Chemical Reagent Co. Ltd. (Shanghai), Eu_2O_3 were purchased from Science and Technology Parent Company of Changchun Institute of Applied Chemistry, and $BaBr_2$ were purchased from Alfa Aesar, USA. All chemicals and materials were used directly without further purification.

In a typical preparation process, the stoichiometric raw materials were mixed thoroughly with a little ethanol, and then were ground for more than 1 hour in an agate mortar with pestle. Next, the mixtures were put into an oven (80℃) for 2 hours. This dried powder precursors were transferred into aluminum oxide crucibles and preheated at 500℃ for 4 hours in air. After being ground, the preheated powders were collected into aluminum oxide crucibles again and sintered in the horizontal tube furnace at 820-900℃ for 7-15 hours under a reduced atmosphere of H_2 (10%)–N_2 (90%). During the sintering process, an intermittent grinding is necessary. When the furnace slowly cooled to room temperature, the obtained powders were ground again. Finally, the resulting phosphor products were harvested undergoing a dealt with deionized water and dried at 80℃.

Characterization. The finely ground powders were used in all measurements. The crystal structure and phase purity of the as-prepared samples were characterized by X-ray powder diffractometer (XRD), which were performed on a D8 Focus diffractometer at as canning rate of 1 ^{o} min^{-1} in the 2θ range from 5^{o} to 120^{o} with Ni-filtered Cu-Kα (λ = 1.540598 Å). XRD Rietveld profile refinements of the structural models and texture analysis were performed with the use of General Structure Analysis System (GSAS) software. The starting model was built with crystallographic data taken from $Ba_2B_5O_9X$[26-27] and $NaBa_4(AlB_4O_9)_2X_3$ (X = Cl, Br).[24] The morphologies, energy-dispersive X-ray spectrum (EDS) and elemental mapping analysis of the samples were inspected using a field emission scanning electron microscope (FE-SEM, S-4800, Hitachi). The photoluminescence excitation (PLE) and emission (PL) spectra were measured by fluorescence spectrometer (Fluoromax-4P, Horiba Jobin Yvon, New Jersey, U.S.A.) equipped with a 450 W xenon lamp as the excitation source, and both excitation and emission spectra were set up to be 1.0 nm with the width of the monochromator slits adjusted as 0.50 nm. The thermal stability of luminescence properties was measured by Fluoromax-4P spectrometer connected a heating equipment (TAP-02). XANES of Eu L_3 edge was recorded with a wiggler beamline BL17C at National Synchrotron Radiation Research Center (NSRRC) in Hsinchu, Taiwan. The diffuse reflectance spectra (DRS) were measured by UV-Visible diffuse reflectance spectroscopy UV-2550PC (Shimadzu Corporation, Japan). The photoluminescence decay curves were obtained from a Lecroy Wave Runner 6100 Digital Osilloscope (1 GHz) using a tunable laser (pulse width = 4 ns, gate = 50 ns) as the excitation (Contimuum Sunlite OPO). The Commission

Internationale de l'Eclairage chromaticity color coordinates, color rendering index (Ra), and CCT of WLED devices were measured by Starspec SSP6612.

■ RESULTS AND DISCUSSION

Crystal structure and lattice parameters.

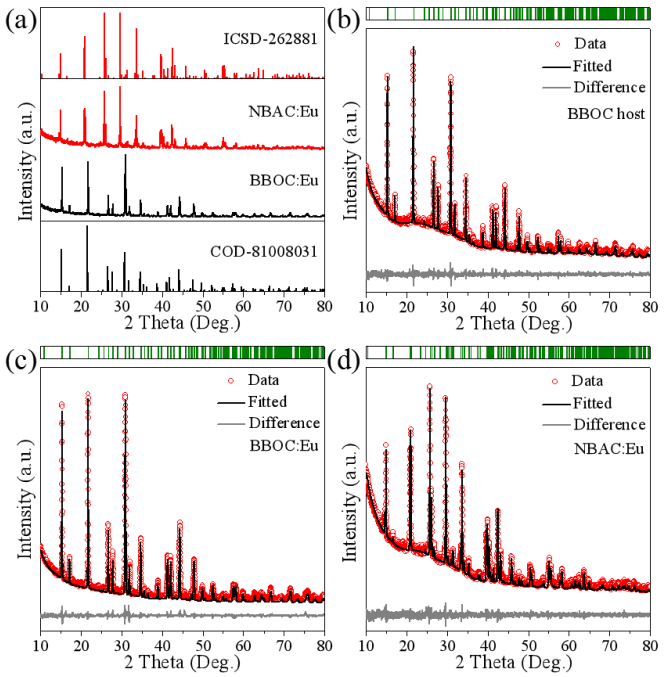

Figure 1. (a) XRD patterns of BBOC:Eu and NBAC:Eu, the standard cards are $Ba_2B_5O_9Cl$ (COD No. 81008031) and $NaBa_4(AlB_4O_9)_2Cl_3$ (ICSD No. 262881). The Rietveld refinement of XRD patterns for (b) BBOC host, (c) BBOC:Eu, (d) NBAC:Eu via GSAS software.

Powder XRD patterns and Rietveld refinements of the studied samples are used to confirm the phase purity and analyze the crystal structure. Figure 1 shows the typical XRD data of BBOC:Eu and NBAC:Eu samples. It needs to be pointed out that the above samples were prepared in the same experimental condition with the same amount of Na_2CO_3. Seen from the Figure 1(a), the sample without Al-doping matches well with the standard card of $Ba_2B_5O_9Cl$ phase (COD No. 81008031), revealing that the Na_2CO_3 only plays the role of flux. When using Al^{3+} ions replace part of B^{3+} ions, all the diffraction peaks are indexed as $NaBa_4(AlB_4O_9)_2Cl_3$ phase (ICSD No. 262881). Therefore, the Na_2CO_3 simultaneously plays the roles of flux and reactant with the introduction of Al^{3+} ions. Besides, Rietveld refinement is used to further affirm the phase purity of as-prepared phosphors, and the results are presented in Figure 1(b)-(d). The samples without Al element were refined with $Ba_2B_5O_9Cl$ as template, which crystallize in orthorhombic phase (Pnn2). While the Al^{3+}-substitution sample is refined with using $NaBa_4(AlB_4O_9)_2Cl_3$ as template, crystallizing in tetragonal phase ($P4_2nm$). The accredited refinement parameters for BBOC host (R_{wp} = 5.75%, R_p = 3.47%, χ^2 = 2.818), BBOC:Eu (R_{wp} = 7.09%, R_p = 4.03%, χ^2 = 4.061) and NBAC:Eu (R_{wp} = 5.49%, R_p = 3.40%, χ^2 = 2.379) indicate that the as-prepared samples maintain the pure phases and form a solid-solution. Meanwhile, the lattice parameters of BBOC:Eu (a = 11.5491(4) Å, b = 11.60042(24) Å, c = 6.66599(21) Å, V = 893.07(4) Å^3) are little smaller than those of BBOC host (a = 11.62360(24) Å, b = 11.57535(30) Å, c = 6.67996(17) Å, V = 898.77(4) Å^3), demonstrating that the Eu^{2+} ions have been successfully doped in BBOC matrix by occupying Ba^{2+} ions sites due to the smaller Eu^{2+} ions (r = 1.30, CN = 9) than that of Ba^{2+} ions (r = 1.47, CN = 9).

According to the refinement results, it is found that both of BBOC and NBAC present highly symmetric lattice environment, and their crystal structure schematic diagrams are all shown in Figure 2. In BBOC host, two $[BO_3]$ units and three $[BO_4]$ units connect each other with one O atom along with the c-axis direction, forming a $[B_5O_{18}]$ group. Subsequently, the $[B_5O_{18}]$ groups are interconnected by sharing one O atom, resulting in a three-dimensional frame structure (Figure 2(a)). It is worthwhile to noting that there are many symmetric tunnels for accommodating Ba^{2+} ions and Cl^- ions. There are two kinds of Ba^{2+} sites (marked as Ba1, Ba2) and Cl^- sites (marked as Cl1, Cl2), of which Ba1 and Cl1 co-occupy a tunnel, while Ba2 and Cl2 co-occupy another tunnel. When one third $[BO_4]$ units are substituted by $[AlO_4]$ units, the lattice will expand, and thus Na^+ ions have to enter the Cl1 tunnels. Simultaneously, Ba1 ions are driven into Cl2 tunnels. The schematic substitution process for $[BO_4] \rightarrow [AlO_4]$ is depicted in Figure 2(b). For NBAC host (Figure 2(c)), there exist two Cl^- sites, one Ba^{2+} sites and one Na^+ sites. Meanwhile, the cell properties are $a \neq b \neq c$, $\alpha = \beta = \gamma = 90°$ for BBOC and $a = b \neq c$, $\alpha = \beta = \gamma = 90°$ for NBAC, respectively. For the above two hosts, the slight difference is the length of a and b, which is ascribed to the different distribution for Ba^{2+} ions and Na^+ ions. From c-axis direction, Ba2—O bond length decide the cell parameter a value, and

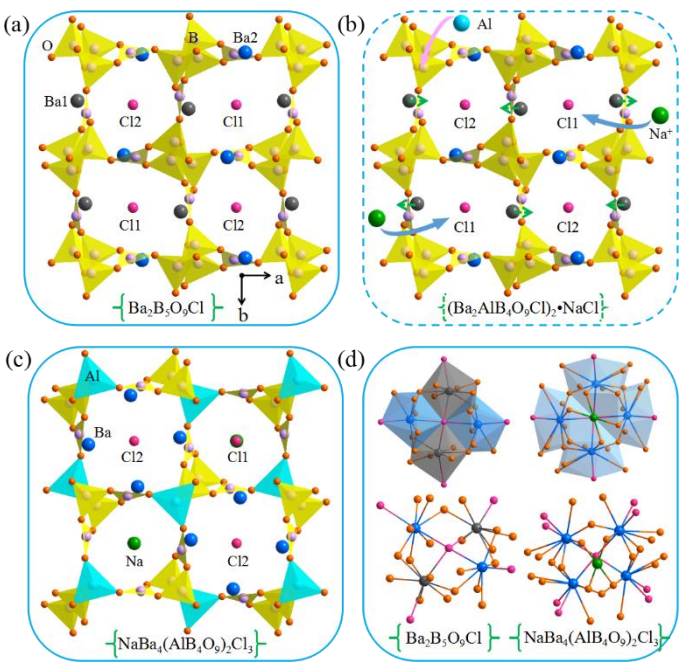

Ba1—O bond length assign the cell parameter b value. Since the different bond length of Ba1—O

Figure 2. The crystal structure schematic diagram along c-axis direction of (a) BBOC, (b) the intermediate process of the phase transformation from BBOC to NBAC and (c) NBAC. (d) The connection of Ba polyhedrons and Na polyhedrons. Where gray, blue, green, cyan, purple, pink, orange spheres represent Ba1 atoms, Ba2 atoms, Na atoms, Al atoms, B atoms, O atoms, and Cl atoms, respectively.

and Ba2—O, $a \neq b$ in BBOC. While only one Ba—O bond length exists in NBAC, so it could be deduced to be $a = b$. In conclusion, the phase transformation between BBOC and NBAC could occur by part cation substitution. Finally, the relationship between Ba^{2+} and Na^{+} polyhedrons for BBOC and NBAC is exhibited in Figure 2(d). For BBOC, the two kinds of Ba^{2+} ions coordinate with seven O atoms and two Cl atoms, two Ba1 polyhedrons and two Ba2 polyhedrons connect as a centrosymmetric flower-like structure by sharing edge and triangle. For NBAC, Ba^{2+} ions coordinate with seven O atoms and three Cl atoms, while Na+ ions coordinate with four O atoms and one Cl atoms. Four Ba polyhedrons form a symmetric flower-like structure with the Na polyhedron locating into the center. Because of the similar ions radius of Eu^{2+} ions, Ba^{2+} ions and Na+ ions, Eu^{2+} ions are considered to randomly occupy Ba^{2+} ions and Na^{+} ions sites.

Luminescence properties

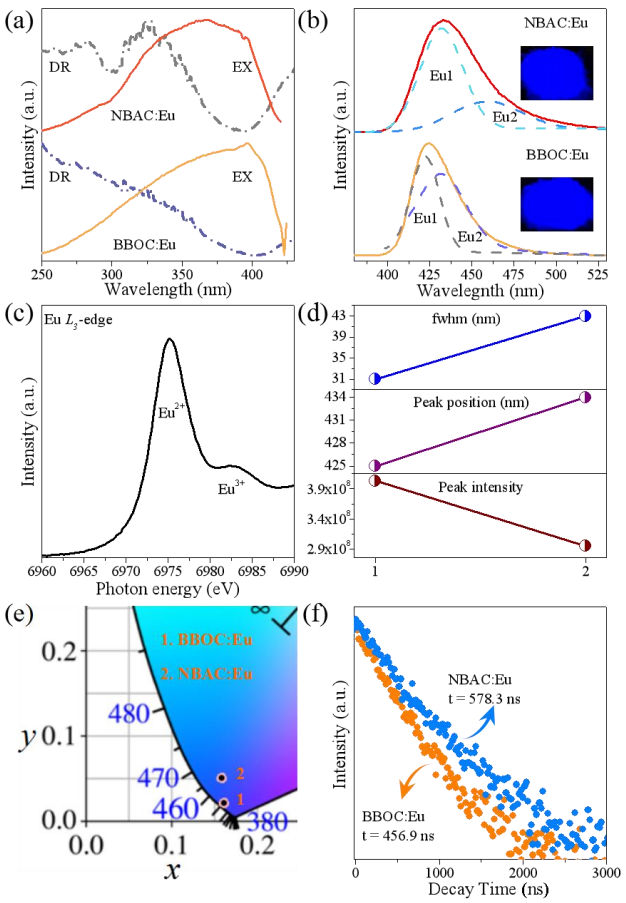

Figure 3. (a) The normalized photoluminescence excitation (PLE) spectra and diffuse reflectance (DR) spectra of BBOC:Eu and NBAC:Eu samples. (b) The normalized photoluminescence emission (PL) spectra with the Gaussian fitting curves of BBOC:Eu and NBAC:Eu samples, the insets are the photographs of as-prepared samples under 365 nm UV lamp. (c) The Eu L_3-edge X-ray absorption near edge structure (XANES) spectra of BBOC:Eu. (d) The fwhm, emission peak and emission intensity of BBOC:Eu and NBAC:Eu. (e) The CIE chromaticity diagram of BBOC:Eu and NBAC:Eu samples. (f) The luminescence life decay curves monitored at λ_{ex} = 365 nm and λ_{em} =430 nm of BBOC:Eu and NBAC:Eu samples.

Because of the highly symmetric lattice structure, the fascinating luminescence properties of as-prepared phosphors are expected and investigated in detail. Figure 3 systematically depicts the photoluminescence properties of the as-prepared phosphor samples. Commonly, a broad band gap for host is beneficial to achieve an efficient doping of rare earth ions. Therefore, the band gap of BBOC host is firstly determined by the following equation based on the corresponding diffuse reflectance (DR):[28-31]

$$[F(R)hv]^{1/2} = A(hv - Eg), F(R) = (1-R)^2 / 2R \quad (1)$$

where A represents the absorption constant, Eg is the optical band gap, hv represents the photon energy, F(R) is the absorption, and R is the reflectance (%) coefficient, respectively. The calculated Eg value for BBOC host is 3.50 eV, illustrating that this host is an appropriate matrix for rare earth luminescence. Figure 3(a) shows the photoluminescence excitation (PLE) spectra of BBOC:Eu and NBAC:Eu samples monitored at the optimal emission wavelength (solid lines). Obviously, a broad absorption band from 250 nm to 430 nm could be observed, which matches the near-UV LED chip well for the application in WLEDs. What's more, the excitation peaks of the two samples are evidently different, the peak position of BBOC:Eu locates at 397 nm, and that of NBAC:Eu situates at 365 nm, indicating the different lattice environment of Eu^{2+} ions in the two matrixes. In addition, the dash lines in Figure 3(a) are the diffuse reflectance (DR) spectra of BBOC:Eu and NBAC:Eu samples, which have strong absorption in 325-430 nm region due to the $4f^7 \rightarrow 4f^6 5d$ transitions of Eu^{2+} ions. The consequences are basically consistent with the PLE results. When monitoring with the respective optimal excitation wavelength, both BBOC:Eu and NBAC:Eu phosphors present highly efficient blue emission, and its photoluminescence emission (PL) spectra are recorded in Figure 3(b). The PL spectrum of BBOC:Eu consists of an asymmetric narrow band from 400 nm to 475 nm centered at 424 nm, which can be deconvoluted to two Gaussian peaks, indicating that there are two independent luminescence centers (marked as Eu1 and Eu2). The emission peaks of Eu1 and Eu2 are determined to be 421 nm and 431 nm, respectively. Compared with BBOC:Eu, the NBAC:Eu presents slightly broader blue-emitting band and the peak position shifts to longer wavelength direction. Simultaneously, the emission band of NBAC:Eu could also be divided into two Gaussian peaks with the maximum values at 432 nm and 459 nm (Figure 3(b)). The corresponding luminescence photos of the studied samples shown in the inset of Figure 3(b) gives further evidence for the highly efficient and pure blue emission.

Figure 3(c) presents the Eu L_3-edge X-ray absorption near edge structure (XANES) spectra of BBOC:Eu phosphor, there are two evident peaks locating at 6975 eV and 6983 eV, which are assigned to the electron transitions of $2p_{3/2}$ - $5d$ in Eu^{2+} and Eu^{3+}, respectively. The result demonstrates that Eu

almost exists in the form of +2 in BBOC matrix and only traces trivalent europium can be observed, which also confirms the highly efficient blue emission of Eu^{2+} in the current host. The comparison of fwhm, peak position and peak intensity for BBOC:Eu and NBAC:Eu are summarized in Figure 3(d). Under the same excitation conditions, BBOC:Eu possesses the stronger luminescence intensity than NBAC:Eu , which is possibly attributed to the slight lattice distortion due to the part $[BO_4] \rightarrow [AlO_4]$ substitution. Moreover, due to the incorporation of $[AlO_4]$ units, the expand of $[B_5O_{18}]$ lattice result in the neighboring Ba^{2+}/Na^{+} lattice contracts. Therefore, the emission peak position of NBAC:Eu shows a slight longer wavelength (433 nm) than that of BBOC:Eu (424 nm). Especially, it is noteworthy that ultra-narrow fwhms are obtained in the PL spectra of BBOC:Eu (31 nm) and NBAC:Eu (43 nm) phosphors, both of which are narrower than the commercial available BAM:Eu^{2+} phosphors (fwhm = 52 nm). To our best knowledge, the 31 nm fwhm of BBOC:Eu samples is the narrowest one among the reported Eu^{2+} or Ce^{3+}-doped blue-emitting phosphors. These ultra-narrow fwhms of the reported phosphors also imply the possibly high-purity blue emission. In order to evaluate the color purity of the as-prepared samples, the CIE chromaticity coordinates were firstly calculated through its emission spectra. The calculated CIE color coordinate values are (0.1613, 0.0212) for BBOC:Eu and (0.1585, 0.0504) for NBAC:Eu, respectively. Obviously, the color coordinate of BBOC:Eu almost close to the limit of blue and violet intersection area in the 1931 CIE color coordinate diagram. A slight red shift from blue-violet to blue appear, which also results from the cation substitution of B^{3+} ions for Al^{3+} ions. Then, the color purity of the two samples could be calculated with the following equation:[24, 32]

$$\text{Color purity} = \frac{\sqrt{(x-x_i)^2+(y-y_i)^2}}{\sqrt{(x_d-x_i)^2+(y_d-y_i)^2}} \times 100\% \quad (2)$$

where (x, y) represent the CIE color coordination of as-prepared samples and commercial BAM:Eu^{2+} phosphor, (x_i, y_i) is the white light source with CIE color coordinate (0.3333, 0.3333) in the reported work, and (x_d, y_d) is the color coordinate corresponding to the dominant wavelength of the light source. The finally calculated color purities are 97.3% for BBOC:Eu and 91.1% for NBAC:Eu. The as-prepared samples all presented superior color purity, especially that of BBOC:Eu even much higher than the commercial BAM:Eu^{2+} phosphor (91.3%) in previous reports.[25] The high color purity properties of the two phosphors could support the promising application in backlit display area. In addition, Figure 3(f) presents the luminescence life decay curves monitored at λ_{ex} = 365 nm and λ_{em} = 430 nm of BBOC:Eu and NBAC:Eu samples. Although two Ba^{2+} (Na^{+}) sites were found in BBOC and NBAC by Rietveld refinement, the decay curves could be successfully fitted using monoexponential equation:

$$I(\tau) = I_0 + A * \exp(-\tau / t) \quad (3)$$

where $I(\tau)$ and I_0 are the luminescence intensities at time τ, A is fitting constant; and t represents the decay time of the exponential components. This result implies the Eu^{2+} ions will mainly occupy one Ba^{2+} sites. The fitted decay time increases from 456.9 ns to 578.3 ns with the replacement of $[BO_4]$ by $[AlO_4]$, also confirming the previous red-shifted emission.

According to the experimental results, a probable mechanism for ultra-narrow blue emission and slight spectral red-shift is proposed as follows: Both BBOC and NBAC have highly symmetric lattice structure, which provide the highly symmetric and rigid coordination environment for Eu^{2+} ions. This not only decreases the distribution of Eu^{2+} emission at different cation sites but also decreases the Eu^{2+} emission due to the lattice distortion. Thus, the extremely narrow fwhms of Eu^{2+} emission could be achieved. Moreover, the fwhm of BBOC:Eu is much narrower than that of NBAC:Eu, which should be attributed to the local lattice expand through partly replacing $[BO_4]$ by $[AlO_4]$. Since there are two types of Ba^{2+} sites in BBOC both coordinated with seven O atoms and two Cl atoms for Eu^{2+}-occupation, and the average bonds of two $[BaO_7Cl]$ polyhedrons are almost similar. Eu1 and Eu2 are randomly assigned to the two Ba^{2+} sites (Figure 3(b)), and

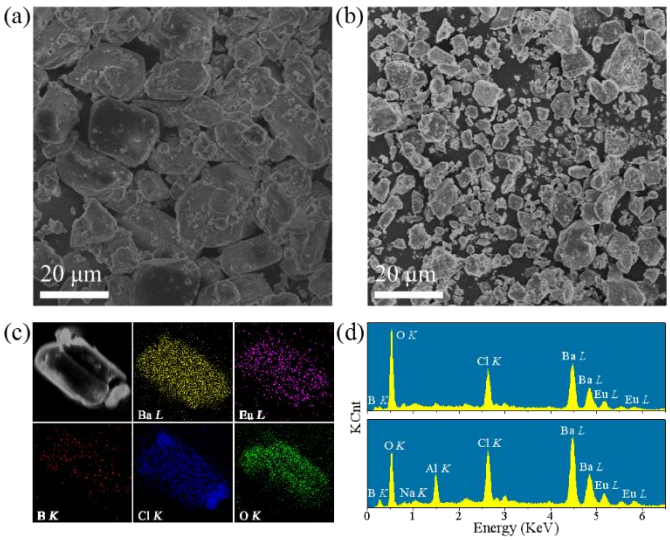

mainly generate one kind of Eu^{2+} emission. However, for NBAC, $[BaO_7Cl_2]$ and $[NaO_4Cl]$ polyhedrons are both suitable for Eu^{2+}-doping, but the average bond lengths of the two polyhedrons have large difference due to the ions radius of Ba^{2+} ions are 1.52 Å for CN = 10 and Na^{+} ions are 1.00 Å for CN = 5. After Eu^{2+} ions entering into the two sites, its fwhm is widened. That is why the final emission band of BBOC:Eu shows more narrower than that of NBAC:Eu.

Figure 4. The SEM images of (a) BBOC:Eu and (b) NBAC:Eu samples. (c) The SEM element mapping images of the representative BBOC:Eu sample. (d) The EDS data of BBOC:Eu and NBAC:Eu samples.

It is known that homogeneous morphology and size plays an important effect on improving luminescence intensity and efficiency of phosphor materials.[33] Figure 4 shows the SEM images and element analysis of BBOC:Eu and NBAC:Eu powders. In the same magnification condition, the as-prepared BBOC:Eu shows homogeneous columnar particle around 20 μm, while NBAC:Eu consists of irregular and inhomogeneous particles in the size range of 1-20 μm. Usually, the more homogeneous particles are, the stronger emission intensity gets due to the decrease of surface defects. So it is reasonable to deduce that the BBOC:Eu has a better luminescence intensity that NBAC:Eu, as confirmed by Figure 3(d). Finally, Figure 4(c) and (d) show the mapping images and EDS data

Table 1. Crystallographic Data for Cl-series (BBOC:Eu, NBAC:Eu) and Br-series (BBOB:Eu, NBAB:Eu) Phosphors Based on the Rietveld Refinements.

Samples	Symmetry	Space Group	*a* (Å)	*b* (Å)	*c* (Å)	V (Å^3)
BBOC host	orthorhombic	Pnn2	11.6236(24)	11.5754(30)	6.6799 (17)	898.77(4)
BBOC:Eu	orthorhombic	Pnn2	11.5491(4)	11.6004(24)	6.6659 (21)	893.07(4)
NBAC:Eu	tetragonal	P4$_2$nm	12.0723(25)	12.07223(25)	6.8247(17)	994.62(4)
BBOB:Eu	orthorhombic	Pnn2	11.6728(7)	11.5906(7)	6.6493(5)	899.60(1)
NBAB:Eu	tetragonal	P4$_2$nm	12.1892(17)	12.1892(17)	6.8324(12)	1015.14(3)

of BBOC:Eu sample. It could be observed that Ba, Eu, B, Cl, O elements uniformly distribute in the particles. Furthermore, the average composition of Eu^{2+}/Ba^{2+} is determined to be 10.2% (10 points were collected at different locations) for BBOC:Eu sample, which is consistent with the nominal Eu^{2+}/Ba^{2+} value.

Except for the Eu^{2+}-doped chlorinated (alumino)borate systems, larger Br^- ions are designed to substitute the smaller Cl^- for exploring novel optical materials. It is delighted that the as-prepared Br-series samples (named as BBOB:Eu and NBAB:Eu) have the same crystal structure and regularity with Cl-series samples (BBOC, NBAC), respectively. There also exists phase transformation from BBOB to NBAB when some Al^{3+} ions occupy B^{3+} sites. The Rietveld refinements of XRD data are plotted in Figure 5, the available reliability factor of BBOB:Eu (R_{wp} = 7.05%, R_p = 5.24%, χ^2 = 3.081) and NBAB:Eu (R_{wp} = 6.15%, R_p = 4.54%, χ^2 = 2.954) certificate the formation of pure phase and good crystallization. All the lattice parameter of Cl-series and Br-series samples refined by GSAS software are summarized in Table 1.

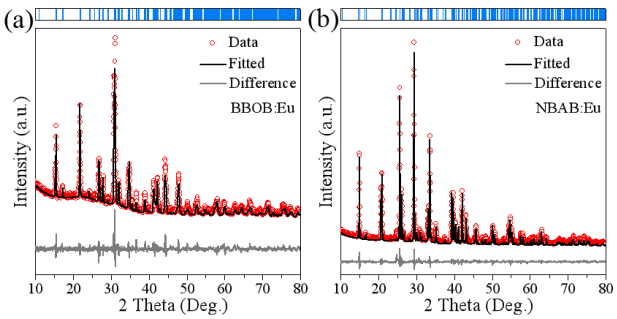

Figure 5. The Rietveld refinement of XRD data for (a) BBOB:Eu sample, (b) NBAB:Eu sample.

Figure 6 demonstrates the luminescence properties of BBOB:Eu and NBAB:Eu samples. The PLE spectra monitoring at 436 nm show a similar trend with the Cl-series plotted in Figure 3(a), indicating that the as-prepared phosphors have strong absorption in near-UV region. However, the PL spectra of BBOB:Eu and NBAB:Eu samples are quite different from their corresponding Cl-series samples, respectively. With the substitution of [AlO_4] for [BO_4], the BBOB:Eu and NBAB:Eu samples present the same emitting peak position at 436 nm. Besides, the two samples could be fitted in two gaussian emission peak of Eu1(436 nm) and Eu2 (454 nm). By comparing the emission spectra of BBOB:Eu and NBAB:Eu samples at the same excitation condition, it is clarified that the profile and peak position stay stable, nevertheless, BBOB:Eu have the stronger luminescence intensity than NBAB:Eu, as shown in Figure 6(c). The XANES spectra of BBOB:Eu in Figure 6(d) exhibits that the main peak is ascribed to the electron transition of $2p_{3/2} \rightarrow 5d$ for Eu^{2+}, only minimal peaks belong to Eu^{3+}, elucidating that the emission band stems from the $4f^6 5d \rightarrow 4f^7$ transitions of Eu^{2+} ions.

In order to intuitively compare the photoluminescence properties of the as-prepared Eu^{2+}-doped Cl-series and Br-series samples. Figure 7(a) gathers the PL spectra of $Ba_2B_5O_9X:Eu^{2+}$ and $NaBa_4(AlB_4O_9)_2X_3:Eu^{2+}$ (X = Cl, Br) samples monitoring at 397 nm near-UV light. One hand, the participation of [AlO_4] group slightly low the crystal symmetry of $NaBa_4(AlB_4O_9)_2X_3:Eu^{2+}$, which decreases the luminescence intensity and increases fwhm compared with $Ba_2B_5O_9X:Eu^{2+}$. On the other hand, when part [BO_4] groups are substituted by [AlO_4] groups, the emission peaks of Cl series happen a red-shift, however, that of Br series stay unchanged. The conceivable reason is that the expand of B^{3+}/Al^{3+} sites result in

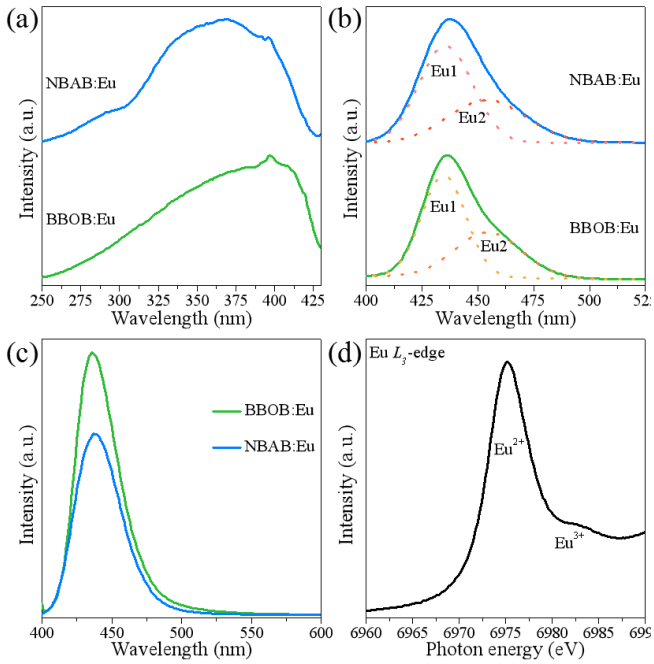

Figure 6. (a) The normalized PLE spectra, (b) The normalized PL spectra and gaussian fitting peaks of BBOB:Eu and NBAB:Eu samples. (c) The comparison of the PL spectra of BBOB:Eu and NBAB:Eu samples. (d) The Eu L_3-edge XANES spectra of the representative BBOB:Eu samples.

The phosphors with narrow fwhm, high efficiency and suitable emission position have a fine application in backlit display and WLEDs. In Figure 7(b), there is a comparison of the CIE color coordinate positions of the as-prepared Cl-series and Br-series samples with Rec. 2020 standard on CIE 1931 color space. The triangle surrounded red dashed lines are the color gamut of the Rec. 2020 display standard, and the blue and yellow triangle regions depict the color gamut by combing the as-prepared blue phosphors and the same green and red phosphors. Gratifyingly, the color gamut achieved by employing the current blue phosphors are almost close to that of Rec. 2020, of which $Ba_2B_5O_9X:Eu^{2+}$ (X = Cl, Br) and NBAB:Eu phosphors reach around 99.5% Rec. 2020, and NBAC:Eu powder contributes up to 96.5% Rec. 2020. Moreover, the color coordinate positions of the as-prepared phosphors are close to the standard blue position (0.131, 0.046). Even the as-prepared BBOC:Eu phosphor (0.162, 0.021) has almost reach the theoretical limit of blue-violet position on the 1931 color diagram, as shown by the magnifying color coordinate region in the inset of Figure 7(b). In addition, Table 2 summaries the excitation peak, emission peak, fwhm, and color purity for the as-prepared Cl-series and Br-series samples and some previous reported blue phosphors. It can be found that the as-prepared blue phosphors in this work present the narrower fwhm than other reported blue phosphors, especially, the BBOC:Eu possesses the most narrow fwhm under the excitation of near-UV light in the all reported $Eu^{2+}/Ce^{3+}/Bi^{3+}$-activated blue phosphors (Table 2). In other words, the as-prepared blue phosphors are remarkable materials for backlit display in WLEDs.

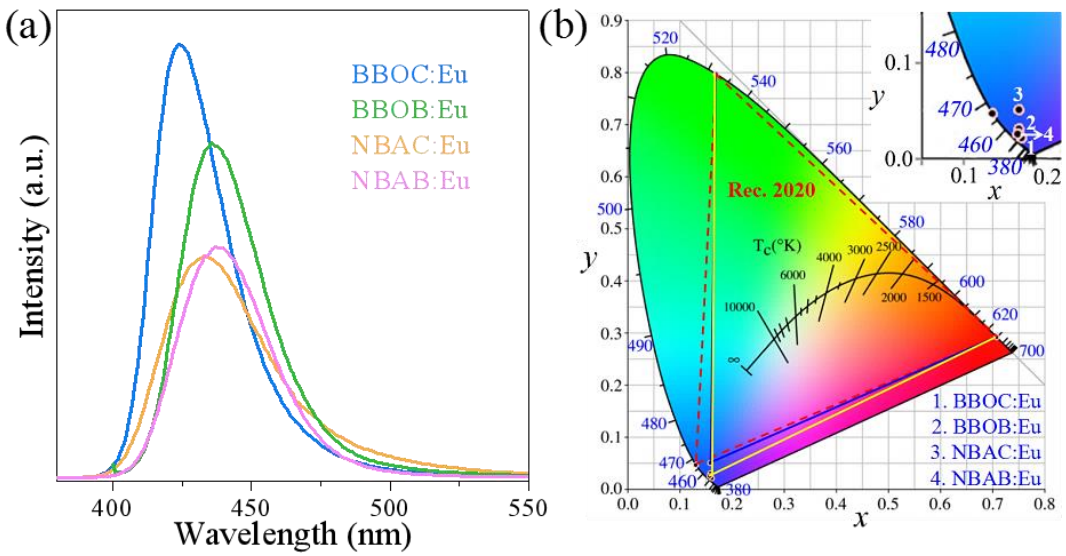

Figure 7. (a) The PL spectra of $Ba_2B_5O_9X:Eu^{2+}$ and $NaBa_4(AlB_4O_9)_2X_3:Eu^{2+}$ (X = Cl, Br) samples. (b) CIE coordination diagram of the as-prepared $Ba_2B_5O_9X:Eu^{2+}$, $NaBa_4(AlB_4O_9)_2X_3:Eu^{2+}$ (X = Cl, Br) on CIE 1931 color space together with the Rec. 2020 standards.

the neighboring Ba^{2+} sites shrinking, corresponding to increase the crystal field splitting of Eu^{2+} 5*d* level, and then the red-shifted emission. But when Cl^- ions are replaced by larger Br^- ions, the tunnels have already been enlarged, so when embedding into Al^{3+} sites, the variation of Ba^{2+}/Na^+ is offset, so the emission shape and position keep constant.

Table 2. The Summary of Excitation Peak, Emission Peak, fwhm, Color Purity for the As-Prepared $Ba_2B_5O_9X:Eu^{2+}$, $NaBa_4(AlB_4O_9)_2X_3:Eu^{2+}$ (X = Cl, Br) Samples and Some Previously Reported $Eu^{2+}/Ce^{3+}/Bi^{3+}$-Activated Blue Phosphors.

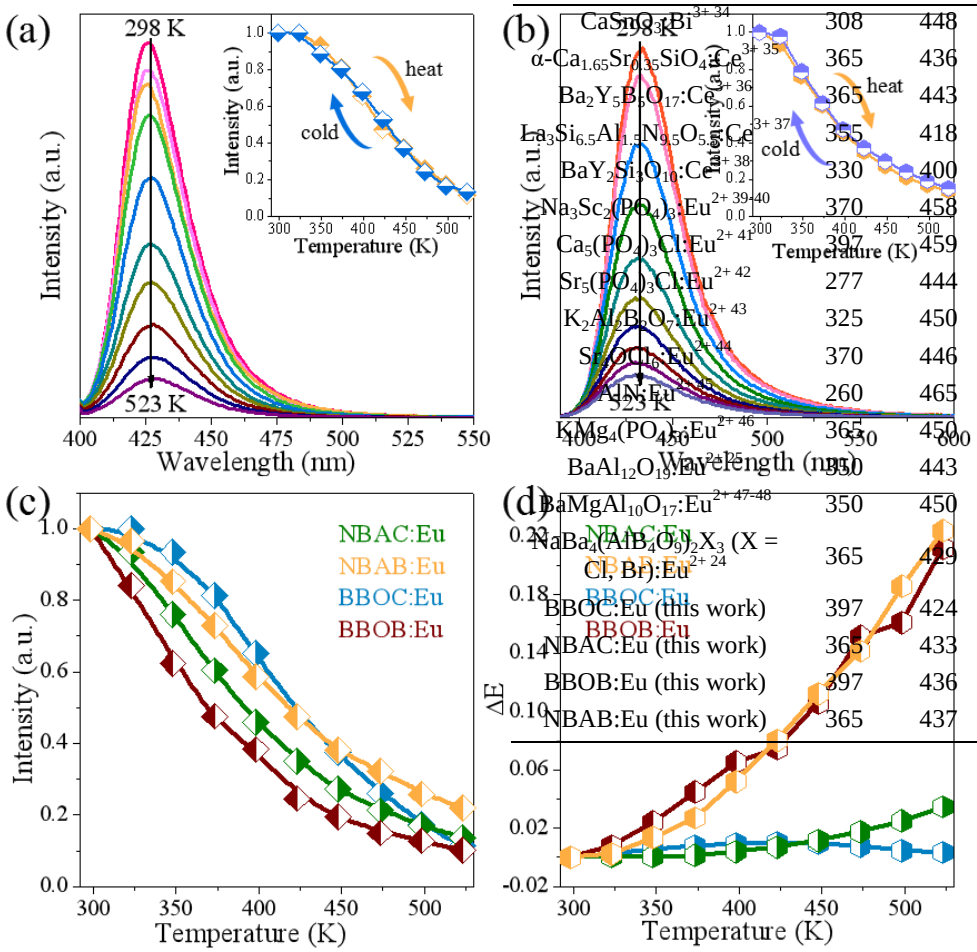

Samples	λ_{ex} (nm)	λ_{em} (nm)	fwhm (nm)	Color purity
$CaSnO_3:Bi^{3+}$ [34]	308	448	—	—
α-$Ca_{1.65}Sr_{0.35}SiO_4$:Ce^{3+} [35]	365	436	75	—
$Ba_2Y_5B_5O_{17}$:Ce^{3+} [36]	365	443	100	—
$La_3Si_{6.5}Al_{1.5}N_{9.5}O_{5.5}$:$Ce^{3+}$ [37]	355	418	68	—
$BaY_2Si_3O_{10}$:Ce^{3+} [38]	330	400	75	—
$Na_3Sc_2(PO_4)_3$:Eu^{2+} [39-40]	370	458	50	89%
$Ca_5(PO_4)_3Cl$:Eu^{2+} [41]	397	459	43	—
$Sr_5(PO_4)_3Cl$:Eu^{2+} [42]	277	444	—	99%
$K_2Al_2B_2O_7$:Eu^{2+} [43]	325	450	53	—
Sr_3OCl_4:Eu^{2+} [44]	370	446	50	—
AlN:Eu^{2+} [45]	260	465	52	—
$KMg_4(PO_4)_3$:Eu^{2+} [46]	365	450	52.2	—
$BaAl_{12}O_{19}$:Eu^{2+} [25]	350	443	52	92%
$BaMgAl_{10}O_{17}$:Eu^{2+} [47-48]	350	450	51.7	91.3%
$NaBa_4(AlB_4O_9)_2X_3$ (X = Cl, Br):Eu^{2+} [24]	365	429	37	98.6%
BBOC:Eu (this work)	397	424	31	97.3%
NBAC:Eu (this work)	365	433	43	91.1%
BBOB:Eu (this work)	397	436	35	95.8%
NBAB:Eu (this work)	365	437	38	97.1%

BBOC:Eu, BBOB:Eu, NBAC:Eu, NBAB:Eu are 460 K, 369 K, 391 K, and 390

Figure 8. The temperature dependent emission spectra of (a) BBOC:Eu and (b) NBAC:Eu from 498 K to 523 K, the insets are the corresponding emission intensity with a heating and cold cycle. (c) The thermal quenching behaviors of Cl-series and Br-series samples at 298 K-523 K. (d) The relationship between CIE color coordinate shift (ΔE) and temperature for Cl-series and Br-series samples.

Because the wording temperature of WLEDs could arrival 373-473 K after long-time operation, thermal quenching property is another significant factor to affect the practical application for phosphor materials.[49-51] Figure 8(a) and 8(b) display the thermal stability properties of the representative BBOC:Eu and NBAC:Eu samples in a heat and cold cycle (298-523 K, with 25 K an internal). It is reasonable to observe that the emission intensities of the representative samples gradually decrease with rising the working temperature due to the non-radiative transition under thermal vibration.[52-53] Although the emission intensity of BBOC:Eu and NBAC:Eu samples only preserve 47.6% and 34.9% of the room temperature intensity at 423 K, respectively, outstandingly demonstrates its excellent physical and chemical stability.Moreover, the thermal quenching behavior of the studied heat reversibility at a and cold cycle phosphors could be further decreased by process optimization. The thermal quenching behavior of all as-prepared phosphors are little serious, the quenching temperature T_{50} (the temperature of the emission intensity at the half of the initial intensity) of

K, respectively, as shown in Figure 8(c), and the subsequent strategy for improving the thermal stability seems to be essential. Figure 8(d) exhibits the CIE shift (ΔE) of Cl-series and Br-series samples from 298 to 523 K following the equation of :[54]

$$\Delta E = \sqrt{(u_t - u_0)^2 + (v_t - v_0)^2 + (w_t - w_0)^2} \quad (4)$$

where $u = 4x/(3 - 2x + 12y)$, $v = 9y/(3 - 2x + 12y)$ and $w = 1 - u - v$. u and v are the chromaticity coordinates in u v uniform color space, x and y are the chromaticity coordinates in CIE 1931 color space, and 0 and t are the chromaticity shift at 298 K and a given temperature. The results show that the CIE color coordinate shifts (ΔE) for Cl series are almost unchanged with temperatures, and it also is better than that of Br series. The low ΔE indicate the color stability of the studied samples with work temperatures, which is beneficial to the stable color output for display devices.

Applications in WLEDs and backlit display

To evaluate the electroluminescence (EL) performance of the as-prepared phosphors, we fabricated blue LEDs and white LEDs with the as-prepared blue phosphors. On the one aspect, the representative NBAC:Eu, BBOC:Eu, BBOB:Eu blue phosphors combine with 370 nm near-UV LED chip to form blue LEDs. On the other aspect, blue NBAC:Eu, BBOC:Eu, BBOB:Eu, green $Ba_3Si_6O_{12}N_2:Eu^{2+}$ and red $CaAlSiN_3:Eu^{2+}$ phosphors were mixed and coated on 370 nm LED chip for the formation of white LEDs. The corresponding EL spectra are recorded in Figure 9. Under a 3.15 V voltage and 20 mA bias current, the fabricated blue LEDs present highly efficient luminescence with excellent color purity even more than 94% for

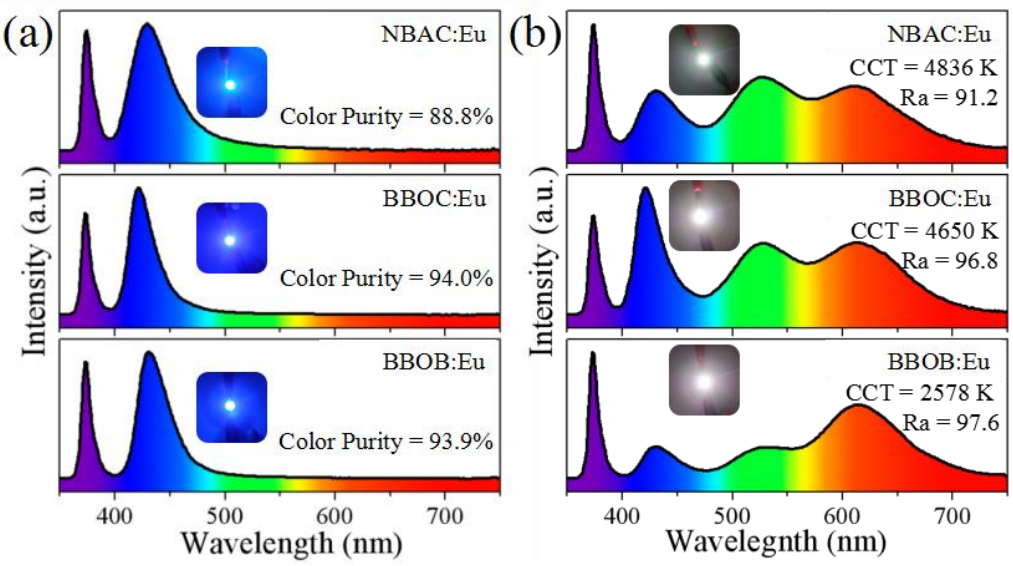

Figure 9. EL spectra of devices fabricated with (a) the representative blue phosphors (NBAC:Eu, BBOC:Eu, BBOB:Eu) + 370 nm LED chip and (b) the representative blue phosphors (NBAC:Eu, BBOC:Eu, BBOB:Eu) + green $Ba_3Si_6O_{12}N_2:Eu^{2+}$ phosphor + red $CaAlSiN_3:Eu^{2+}$ phosphor + 370 nm chip.

$Ba_2B_5O_9X:Eu^{2+}$ (X = Cl, Br) and 88.8% for NBAC:Eu, suggesting greatly potential applications in electronic display devices. In addition, the excellent warm whites with low correlated color temperature (CCT = 2578 - 4836 K), high color rendering index (Ra = 91.2- 97.6) could be gained. These results prove that the as-prepared $Ba_2B_5O_9X:Eu^{2+}$ and $NaBa_4(AlB_4O_9)_2X_3:Eu^{2+}$ (X = Cl, Br) phosphors could be superior candidates for blue-emitting phosphors to applied in near-UV white LEDs.

■ CONCLUSION

In this work, extraordinarily narrow-band blue-emitting $Ba_2B_5O_9X:Eu^{2+}$ and $NaBa_4(AlB_4O_9)_2X_3:Eu^{2+}$ (X = Cl, Br) phosphors were successfully prepared by traditional high temperature solid-state process. Through the Rietveld refinement analysis, the fundamental construction framework and lattice structure of $Ba_2B_5O_9X$ and $NaBa_4(AlB_4O_9)_2X_3$ (X = Cl, Br), are almost the same and highly symmetric. Especially, the highly symmetric lattice environment for Eu^{2+} ions lead to the ultra-narrow emission band (fwhm = 31 - 43 nm, peak position located around 424 - 437 nm) and highly efficient blue emission. Surprisingly, the 31 nm fwhm of BBOC:Eu sample is the narrowest one among the reported rare earth doped blue-emitting phosphors, which realizes a color purity beyond 97%. Moreover, the color gamut surrounded by the color coordinate points of the as-prepared blue phosphors and the standard green and red phosphors are very close to that of Rec. 2020 standards, of which $Ba_2B_5O_9X:Eu^{2+}$ (X = Cl, Br) and NBAB:Eu phosphors could reach to about 99.5% Rec. 2020 standard, and NBAC:Eu phosphor contributes up to 96.5% Rec. 2020 standard. The fabricated blue LEDs present high efficient luminescence with excellent color purity even more than 94% for $Ba_2B_5O_9X:Eu^{2+}$ (X = Cl, Br) and 88.8% for NBAC:Eu. Moreover, the excellent warm white with low corresponding color temperature (CCT = 2578–4836 K), high color rendering index (Ra = 91.2- 97.6) could be gained with the combination of the as-prepared blue phosphors, $Ba_3Si_6O_{12}N_2:Eu^{2+}$ green and $CaAlSiN_3:Eu^{2+}$ red phosphor. Generally, the as-prepared blue emitting phosphors have promising application in backlit display and WLEDs lighting area.

■ ASSOCIATED CONTENT

XRD, EXANES, PLE, PL, Decay curves, Temperature-dependent PL spectra, Refined crystallographic parameters, SEM, EDS, mapping, CIE Color Coordinates, Emission Peaks and fwhm of $Ba_2B_5O_9X:Eu^{2+}$ and $NaBa_4(AlB_4O_9)_2X_3:Eu^{2+}$ (X = Cl, Br) phosphors, Fractional Atomic Coordinates and Isotropic Atomic Displacement Parameters ($Å^2$) of $Ba_2B_5O_9X:Eu^{2+}$ and $NaBa_4(AlB_4O_9)_2X_3:Eu^{2+}$ (X = Cl, Br) phosphors.

■ AUTHOR INFORMATION

Corresponding Author

*Email: ggli@cug.edu.cn
*Email: jlin@ciac.ac.cn
*Email: zycheng@ciac.ac.cn

Notes

The authors declare no competing financial interest.

■ ACKNOWLEDGEMENT

This work was supported by the National Natural Science Foundation of China (Grant Nos. 51672259, 51672265, 21521092, 51750110511), Engineering Research Center of Nano-Geomaterials of Ministry of Education, China University of Geosciences (Wuhan) (No. NGM2016KF002), the National College Students' Innovative Training Program (Nos. 201710491016, 201710491115, 201710491130), the Ministry of Science and Technology of Taiwan (Contract No. MOST 104-2113-M-027-007-MY3), the Key Research Program of Frontier Sciences, CAS (Grant No. YZDY-SSW-JSC018), and projects for science and technology development plan of Jilin province (20170414003GH), and Jiangmen Innovative Research Team Program. the Russian Science Foundation (Grant No. 17-12-01047).

■ REFERENCES

(1) Xia, Z. G.; Liu, Q. L. Progress in Discovery and Structural Design of Color Conversion Phosphors for LEDs. *Prog. Mater. Sci.* **2016**, *84*, 59-117.

(2) Li, G.; Lin, J. Recent Progress in Low-Voltage Cathodoluminescent Materials: Synthesis, Improvement and Emission Properties. *Chem. Soc. Rev.* **2014**, *43*, 7099-7131.

(3) Wang, L.; Xie, R. J.; Suehiro, T.; Takeda, T.; Hirosaki, N. Down-Conversion Nitride Materials for Solid State Lighting: Recent Advances and Perspectives. *Chem. Rev.* **2018**, *118*, 1951-2009.

(4) Feldmann, T. J., Cees R. Ronda, and Peter J. S. Inorganic Luminescent Materials 100 Year of Reasearch and Application. *Adv. Funct. Mater*. **2003**, *13*, 511-516.

(5) George, N. C.; Denault, K. A.; Seshadri, R., Phosphors for Solid-State White Lighting. Annual Review of Materials Research 2013, 43 (1), 481-501.

(6) Terraschke, H.; Wickleder, C. UV, Blue, Green, Yellow, Red, and Small: Newest Developments on Eu(2+)-Doped Nanophosphors. *Chem. Rev*. **2015**, *115*, 11352-11378.

(7) Protesescu, L.; Yakunin, S.; Bodnarchuk, M. I.; Krieg, F.; Caputo, R.; Hendon, C. H.; Yang, R. X.; Walsh, A.; Kovalenko, M. V. Nanocrystals of Cesium Lead Halide Perovskites ($CsPbX_3$, X = Cl, Br, and I): Novel Optoelectronic Materials Showing Bright Emission with Wide Color Gamut. *Nano Lett*. **2015**, *15*, 3692-3696.

(8) Huang, H.; Zhao, F.; Liu, L.; Zhang, F.; Wu, X. G.; Shi, L.; Zou, B.; Pei, Q.; Zhong, H. Emulsion Synthesis of Size-Tunable $CH_3NH_3PbBr_3$ Quantum Dots: An Alternative Route toward Efficient Light-Emitting Diodes. *ACS Appl. Mater. Interfaces* **2015**, *7*, 28128-28133.

(9) Nedelcu, G.; Protesescu, L.; Yakunin, S.; Bodnarchuk, M. I.; Grotevent, M. J.; Kovalenko, M. V. Fast Anion-Exchange in Highly Luminescent Nanocrystals of Cesium Lead Halide Perovskites ($CsPbX_3$, X = Cl, Br, I). *Nano Lett*. **2015**, *15*, 5635-5640.

(10) Song, J.; Li, J.; Li, X.; Xu, L.; Dong, Y.; Zeng, H. Quantum Dot Light-Emitting Diodes Based on Inorganic Perovskite Cesium Lead Halides ($CsPbX_3$). *Adv. Mater.* **2015**, *27*, 7162-7167.

(11) Wang, Y.; Li, X.; Song, J.; Xiao, L.; Zeng, H.; Sun, H. All-Inorganic Colloidal Perovskite Quantum Dots: A New Class of Lasing Materials with Favorable Characteristics. *Adv. Mater*. **2015**, *27*, 7101-7108.

(12) Zhang, X.; Fang, M.-H.; Tsai, Y.-T.; Lazarowska, A.; Mahlik, S.; Lesniewski, T.; Grinberg, M.; Pang, W. K.; Pan, F.; Liang, C.; Zhou, W.; Wang, J.; Lee, J.-F.; Cheng, B.-M.; Hung, T.-L.; Chen, Y.-Y.; Liu, R.-S. Controlling of Structural Ordering and Rigidity of β-SiAlON:Eu through Chemical Cosubstitution to Approach Narrow-Band-Emission for Light-Emitting Diodes Application. *Chem. Mater*. **2017**, *29*, 6781-6792.

(13) Braun, C.; Seibald, M.; Borger, S. L.; Oeckler, O.; Boyko, T. D.; Moewes, A.; Miehe, G.; Tucks, A.; Schnick, W. Material properties and Structural Characterization of $M_3Si_6O_{12}N_2:Eu^{2+}$ (M = Ba, Sr)--A Comprehensive Study on a Promising Green Phosphor for pc-LEDs. *Chem. Eur. J*. **2010**, *16*, 9646-9657.

(14) Li, G.; Lin, C. C.; Chen, W.-T.; Molokeev, M. S.; Atuchin, V. V.; Chiang, C.-Y.; Zhou, W.; Wang, C.-W.; Li, W.-H.; Sheu, H.-S.; Chan, T.-S.; Ma, C.; Liu, R.-S. Photoluminescence Tuning via Cation Substitution in Oxonitridosilicate Phosphors: DFT Calculations, Different Site Occupations, and Luminescence Mechanisms. *Chem. Mater*. **2014**, *26*, 2991-3001.

(15) Kang, F.; Zhang, H.; Wondraczek, L.; Yang, X.; Zhang, Y.; Lei, D. Y.; Peng, M. Band-Gap Modulation in Single Bi^{3+}-Doped Yttrium–Scandium–Niobium Vanadates for Color Tuning over the Whole Visible Spectrum. *Chem. Mater*. **2016**, *28*, 2692-2703.

(16) Xia, Z.; Liu, G.; Wen, J.; Mei, Z.; Balasubramanian, M.; Molokeev, M. S.; Peng, L.; Gu, L.; Miller, D. J.; Liu, Q.; Poeppelmeier, K. R. Tuning of Photoluminescence by Cation Nanosegregation in the $(CaMg)_x(NaSc)_{1-x}Si_2O_6$ Solid Solution. *J. Am. Chem. Soc*. **2016**, *138*, 1158-1161.

(17) Xia, Z.; Ma, C.; Molokeev, M. S.; Liu, Q.; Rickert, K.; Poeppelmeier, K. R. Chemical Unit Cosubstitution and Tuning of Photoluminescence in the $Ca_2(Al_{(1-x)}Mg_{(x)})(Al_{(1-x)}Si_{(1+x)})O_7:Eu^{(2+)}$ Phosphor. *J. Am. Chem. Soc*. **2015**, *137*, 12494-12497.

(18) Wang, Y.; Ding, J.; Wang, Y. $Ca_{2-x}Y1+xZr_{2-x}Al_{3+x}O_{12}:Ce^{3+}$: Solid Solution Design toward the Green Emission Garnet Structure Phosphor for Near-UV LEDs and Their Luminescence Properties. *J. Phys. Chem. C* **2017**, *121*, 27018-27028.

(19) Zhang, J.; Zhang, J.; Zhou, W.; Ji, X.; Ma, W.; Qiu, Z.; Yu, L.; Li, C.; Xia, Z.; Wang, Z.; Lian, S. Composition Screening in Blue-Emitting $Li_4Sr_{1+x}Ca_{0.97-x}(SiO_4)_2:Ce^{(3+)}$ Phosphors for High Quantum Efficiency and Thermally Stable Photoluminescence. *ACS Appl. Mater. Interfaces* **2017**, *9*, 30746-30754.

(20) K. B. Kim, Y. I. K., H. G. Chun, T. Y. Cho,; J. S. Jung, J. G. K. Structural and Optical Properties of $BaMgAl_{10}O_{17}:Eu^{2+}$ Phosphor. *Chem. Mater*. **2002**, *14*, 5045-5052.

(21) S. S. Lee, H. J. K., S. H. Byeon, J. C. Park,; Kim, D. K. Thermal-Shock-Assisted Solid-State Process for the Production of $BaMgAl_{10}O_{17}$:Eu Phosphor. *Ind. Eng. Chem. Res.* **2005**, *44*, 4300-4303.

(22) Yin, L.-J.; Dong, J.; Wang, Y.; Zhang, B.; Zhou, Z.-Y.; Jian, X.; Wu, M.; Xu, X.; van Ommen, J. R.; Hintzen, H. T. Enhanced Optical Performance of $BaMgAl_{10}O_{17}:Eu^{2+}$ Phosphor by a Novel Method of Carbon Coating. *J. Phys. Chem. C* **2016**, *120*, 2355-2361.

(23) Yin, L. J.; Liang, Y. L.; Zhang, S. H.; Wang, M.; Li, L.; Xie, W. J.; Zhong, H.; Jian, X.; Xu, X.; Wang, X.; Deng, L. J. A novel Strategy to Motivate the Luminescence Efficiency of a Phosphor: Drilling Nanoholes on the Surface. *Chem. Commun*. (Camb) **2018**.

(24) Lian, Z.; Yan, Q. Eu^{2+}-Doped $NaBa_4(AlB_4O_9)_2X_3$(X = Cl, Br) Phosphors with Intense Two-Center Blue Emission and High Color Purity for n-UV Pumped White Light-Emitting Diodes. *J. Mater. Chem. C* **2016**, *4*, 7959-7965.

(25) Wei, Y.; Cao, L.; Lv, L.; Li, G.; Hao, J.; Gao, J.; Su, C.; Lin, C. C.; Jang, H. S.; Dang, P.; Lin, J. Highly Efficient Blue Emission and Superior Thermal Stability of $BaAl_{12}O_{19}:Eu^{2+}$ Phosphors Based on Highly Symmetric Crystal Structure. *Chem. Mater*. **2018**, *30*, 2389-2399.

(26) Zheng, J. ; Kang, F.; Cao, R.; Ma, Z.; Dong, G.; Qiu, J.; Xu, S. Broadband NIR Luminescence from a New Bismuth Doped $Ba_2B_5O_9Cl$ Crystal: Evidence for the Bi0 Model. *OPTICS EXPRESS*, **2012**, 20 22569.

(27) Thakare, D. S.; Omanwar, S. K.; Muthal, P. L.; Dhopte, S. M.; Kondawar, V. K.; Moharil, S. V. UV-Emitting Phosphors: Synthesis, Photoluminescence and Applications. *Phys. Status. Solid. (a)* **2004**, *201*, 574-581.

(28) Tauc, R. Grigorovici, A. V. Optical Properties and Electronic Structure of Amorphous Gemanium. *phys. start.* **1966**, *15*, 627-637.

(29) Liu, L.; Yang, Y.; Jing, Q.; Dong, X.; Yang, Z.; Pan, S.; Wu, K. $K_5Ba_{10}(BO_3)_8F$: A New Potassium Barium Borate Fluoride with a Perovskite-Like Structure. *J. Phys. Chem. C* **2016**, *120*, 18763-18770.

(30) Wang, X. M.; Zhang, X.; Ye, S.; Jing, X. P. A Promising Yellow Phosphor of Ce^{3+}/Li^{+}Doped $CaSiN_{(2-2delta/3)}O_{delta}$ for Pc-LEDs. *Dalton Trans.* **2013**, *42*, 5167-5173.

(31) Deng, T. T.; Song, E. H.; Sun, J.; Wang, L. Y.; Deng, Y.; Ye, S.; Wang, J.; Zhang, Q. Y. The Design and Preparation of the Thermally Stable, Mn^{4+}ion Activated, Narrow Band, Red Emitting Fluoride $Na_3GaF_6:Mn^{4+}$ for Warm WLED Applications. *J. Mater. Chem. C* **2017**, *5*, 2910-2918.

(32) Du, P.; Yu, J. S. Photoluminescence and Cathodoluminescence Properties of Eu^{3+} Ions Activated $AMoO_4$ (A = Mg, Ca, Sr, Ba) Phosphors. *Mater. Res. Bull.* **2015**, *70*, 553-558.

(33) Wan, J.; Zhang, Y.; Wang, Y.; Ma, R.; Wu, Y.; Qiao, X.; Fan, X. Facile Synthesis of Monodisperse $SrAl_2O_4:Eu^{2+}$ Cage-Like Microspheres with an Excellent Luminescence Quantum Yield. *J. Mater. Chem. C* **2018**, *6*, 3346-3351.

(34) Lin, C. C.; Tsai, Y. T.; Johnston, H. E.; Fang, M. H.; Yu, F.; Zhou, W.; Whitfield, P.; Li, Y.; Wang, J.; Liu, R. S.; Attfield, J. P. Enhanced Photoluminescence Emission and Thermal Stability from Introduced Cation Disorder in Phosphors. *J. Am. Chem. Soc.* **2017**, *139*, 11766-11770.

(35) Chen, W. Eu^{2+} and Eu^{3+} Co-Activated $LaAlO_3$ Phosphor: Synthesis and Tuned Luminescence. *Dalton Trans.* **2015**, *44*, 17730-17735.

(36) Im, W. B.; George, N.; Kurzman, J.; Brinkley, S.; Mikhailovsky, A.; Hu, J.; Chmelka, B. F.; DenBaars, S. P.; Seshadri, R. Efficient and Color-Tunable Oxyfluoride Solid Solution Phosphors for Solid-State White Lighting. *Adv. Mater*. **2011**, *23*, 2300-2305.

(37) Wang, C.-Y.; Kate, O. M. t.; Takeda, T.; Hirosaki, N. Efficient and Thermally Stable Blue-Emitting Ce^{3+} Doped $LaAl(Si_{6-z}Al_z)(N_{10-z}O_z)$ (JEM:Ce) Phosphors for White LEDs. *J. Mater. Chem. C* **2017**, *5*, 8295-8300.

(38) Yeh, C. W.; Chen, W. T.; Liu, R. S.; Hu, S. F.; Sheu, H. S.; Chen, J. M.; Hintzen, H. T. Origin of Thermal Degradation of $Sr_{(2-x)}Si_5N_8$:Eu(x) Phosphors in Air for Light-Emitting Diodes. *J. Am. Chem. Soc*. **2012**, *134*, 14108-14117.

(39) Cao, R.; Zhang, J.; Wang, W.; Hu, Q.; Li, W.; Ruan, W.; Ao, H. Synthesis and Luminescence Properties of $CaSnO_3:Bi^{3+}$ Blue Phosphor and the Emission Improvement by Li^{+} ion. *Lumin.* **2017**, *32*, 908-912.

(40) Li, K.; Shang, M.; Lian, H.; Lin, J., Photoluminescence Properties of Efficient Blue-Emitting Phosphor α-$Ca_{1.65}Sr_{0.35}SiO_4:Ce^{(3+)}$: Color Tuning via the Substitutions of Si by Al/Ga/B. *Inorg. Chem.* **2015**, *54*, 7992-8002.

(41) Hermus, M.; Phan, P.-C.; Brgoch, J. Ab Initio Structure Determination and Photoluminescent Properties of an Efficient, Thermally Stable Blue Phosphor, $Ba_2Y_5B_5O_{17}:Ce^{3+}$. *Chem. Mater*. **2016**, *28*, 1121-1127.

(42) Wang, C. Y.; Takeda, T.; Ten Kate, O. M.; Tansho, M.; Deguchi, K.; Takahashi, K.; Xie, R. J.; Shimizu, T.; Hirosaki, N. Ce-Doped $La_3Si_{6.5}Al_{1.5}N_{9.5}O_{5.5}$, a Rare Highly Efficient Blue-Emitting Phosphor at Short Wavelength toward High Color Rendering White LED Application. *ACS Appl. Mater. Interfaces* **2017**, *9*, 22665-22675.

(43) Wang, J.; Zhao, W., Optical Characterization and the Energy Level Scheme for Ce^{3+} -Doped BaY_2 Si_3 O_{10} Blue-Emitting Phosphor. *Lumin.* **2017**, *32*, 285-291.

(44) Wang, X.; Zhao, Z.; Wu, Q.; Wang, C.; Wang, Q.; Yanyan, L.; Wang, Y. Structure, Photoluminescence and Abnormal Thermal Quenching Behavior of Eu^{2+}-Doped $Na_3Sc_2(PO_4)_3$: a Novel Blue-Emitting Phosphor for n-UV LEDs. *J. Mater. Chem. C* **2016**, *4*, 8795-8801.

(45) Kim, Y. H.; Arunkumar, P.; Kim, B. Y.; Unithrattil, S.; Kim, E.; Moon, S. H.; Hyun, J. Y.; Kim, K. H.; Lee, D.; Lee, J. S.; Im, W. B. A Zero-Thermal-Quenching Phosphor. *Nat. Mater.* **2017**, *16*, 543-550.

(46) Wei, Y.; Qi, X.; Xiao, H.; Luo, W.; Yao, H.; Lv, L.; Li, G.; Lin, J. Site-Preferential Occupancy Induced Photoluminescence Tuning in $(Ca,Ba)_5(PO_4)_3Cl:Eu^{2+}$ Phosphors. *RSC Adv.* **2016**, *6*, 43771-43779.

(47) Zheng, J.; Cheng, Q.; Wu, S.; Guo, Z.; Zhuang, Y.; Lu, Y.; Li, Y.; Chen, C. An Efficient Blue-Emitting $Sr_5(PO_4)_3Cl:Eu^{2+}$ Phosphor for Application in Near-UV White Light-Emitting Diodes. *J. Mater. Chem. C* **2015**, *3*, 11219-11227.

(48) Xiao, W.; Zhang, X.; Hao, Z.; Pan, G. H.; Luo, Y.; Zhang, L.; Zhang, J. Blue-Emitting $K_2Al_2B_2O_7:Eu^{2+}$ Phosphor with High Thermal Stability and High Color Purity for Near-UV-Pumped White Light-Emitting Diodes. *Inorg. Chem.* **2015**, *54*, 3189-3195.

(49) Gwak, S. J.; Arunkumar, P.; Im, W. B. A New Blue-Emitting Oxohalide Phosphor $Sr_4OCl_6:Eu^{2+}$ for Thermally Stable, Efficient White-Light-Emitting Devices under Near-UV. *J. Phys. Chem. C* **2014**, *118*, 2686-2692.

(50) Kazuo Inoue, N. H.; Xie，R.-J.; Takeda, T.; Highly Efficient and Thermally Stable Blue-Emitting $AlN:Eu^{2+}$ Phosphor for Ultraviolet White Light-Emitting Diodes. *J. Phys. Chem. C* **2009**, *113* 9392-9397.

(51) Chen, J.; Liu, Y.; Mei, L.; Liu, H.; Fang, M.; Huang, Z. Crystal Structure and Temperature-Dependent Luminescence Characteristics of $KMg_4(PO_4)_3:Eu^{2+}$ Phosphor for White Light-Emitting Diodes. *Sci. Rep.* **2015**, *5*, 9673.

(52) Kim, K.-B.; Y.-I. K.; H.-G. C.; Cho, T.-Y.; Jung, J.-S.; K. J.-G. Structural and Optical Properties of $BaMgAl_{10}O_{17}:Eu^{2+}$ Phosphor. *Chem. Mater.* **2002**, *14*, 5045-5052.

(53) Lee, S.-S.; K., H. J.; Byeon, S.-H.; Park, J.-C.; Kim, D.-K. Thermal-Shock-Assisted Solid-State Process for the Production of $BaMgAl_{10}O_{17}$:Eu Phosphor. *Ind. Eng. Chem. Res.* **2005**, *44*, 4300-4303.

(54) Mao, A.; Zhao, Z.; Wang, Y. Orange Phosphor $Li_2SrSiON_2:Eu^{2+}$ for Blue Light Chip Based Warm White LEDs. *RSC Adv.* **2017**, *7*, 42634-42640.

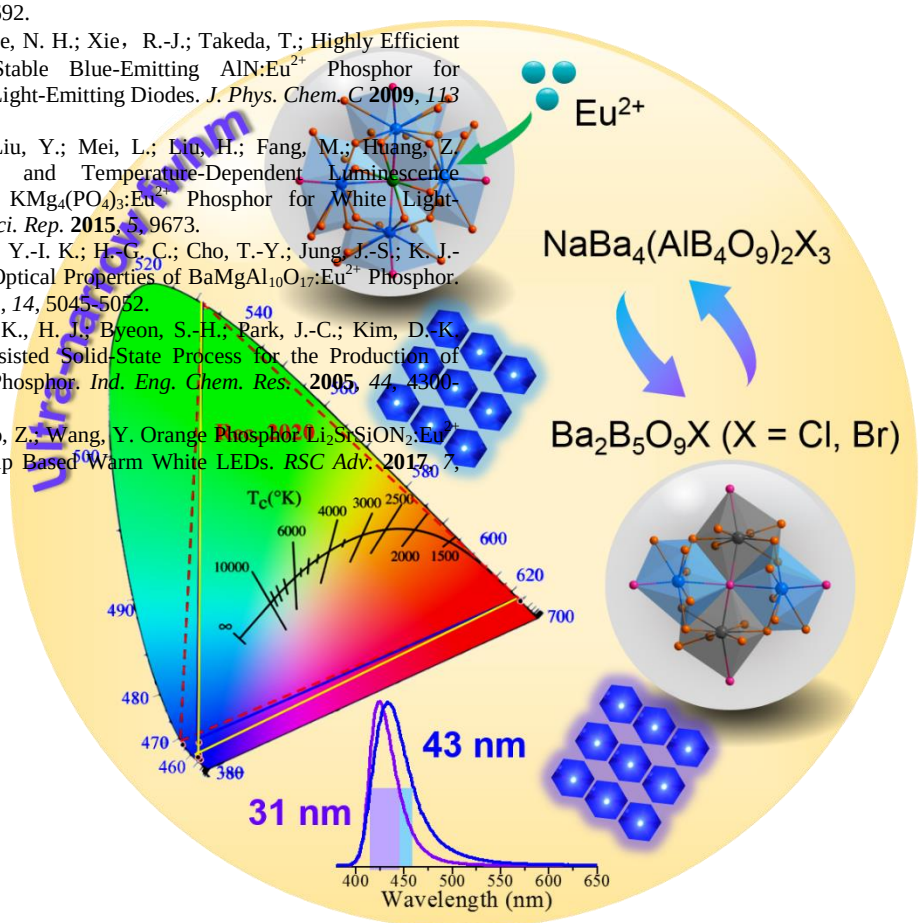

Ultra-narrow band blue emission of Eu^{2+} (fwhm = 31-43 nm) are achieved in halogenated (alumino)borate matrixes due to the highly symmetric lattice structures with the flower-like polyhedrons, of which color gamut could reach the Rec. 2020 display standard by combining the standard green and red phosphors.